Turbine and exhaust ports thermal insulation impact on the engine efficiency and aftertreatment inlet temperature

José Manuel Luján, José Ramon Serrano, Pedro Piqueras, Bárbara Diesel

CMT-Motores Térmicos, Universitat Politècnica de València, Camino de Vera s/n, 46022 Valencia, Spain.

Abstract

Worldwide emission regulations are driven the efforts of the automotive industry to meet challenging targets concerning pollution reduction. Nowadays, advances in exhaust aftertreatment systems are primarily required to achieve regulation requirements within the whole engine operating range. Nevertheless, flow parameters, such as the exhaust gas temperature, must be also addressed. This makes engine calibration a fundamental step, but also leads to reconsider the passive design of the exhaust line as a way to improve the engine efficiency. Under this context, a study has been conducted to explore the benefits of heat losses limitation looking for aftertreatment inlet temperature increase at the same time fuel economy is improved. To do so, a baseline diesel engine has been modeled using a gas dynamic software taking special care of the heat transfer processes in the exhaust. The investigation covers the definition of different strategies for exhaust ports and turbine thermal insulation, which are evaluated in a representative range of steady-state operating conditions. As a first step, the theoretical limits and representative technology solutions are considered for each exhaust region. Then, a combination of the most promising strategies has been computed to provide a comprehensive database and analysis of the potential of passive exhaust heat losses control.

Keywords: Emissions regulation, Diesel engine, Exhaust aftertreatment system, Turbine outlet temperature, Exhaust thermal insulation, Fuel consumption

1. Introduction

Energy policies in the major automotive regions establish air quality standards that impose CO_2 emission targets to reduce the environmental impact of transport activities [1]. To guarantee the compliance with the limits in real driving conditions, the Worldwide Harmonized Light Vehicles Test Procedure (WLTP) was set out in Europe for determining the levels of pollutants, coming progressively into force from September 2017 [2]. In this way, Ko *et al.* [3] presented a study about differences in NO_x emissions between the old and the new test approval cycle that emphasized the need to seize more severe methods to determine real emissions from internal combustion engines.

*Corresponding author. Tel.: +34 96 3877650, fax: +34 96 3877659.
Email address: pedpicab@mot.upv.es (Pedro Piqueras)

New emission regulations are effectively forcing the development of new combustion strategies and improvements in the exhaust aftertreatment systems (EATS) to reduce pollution, looking at the same time for minor or no prejudice on fuel consumption. For instance, Li *et al.* [4] performed investigations on soot emission reduction by including a cooling stage of the recirculated exhaust gas in boosted spark-ignited direct-injection engines, obtaining up to 48% less soot. This decrease is mainly attributed to the dilution effect of the cooled exhaust gas recirculation (EGR) in the mixture, leading to less local rich regions formation. The cooled EGR also causes a lower reaction temperature of pool fires, main responsible for soot formation [5], near the walls.

To assure a good functioning of the aftertreatment devices, their working temperature emerges as the most important variable governing the conversion efficiency [6]. To be specific, the diesel oxidation catalyst (DOC), which is commonly used to oxidize CO and HC emissions as well as NO into NO_2, can work with high conversion efficiency over 200^{o}C [7]. However, to reduce NO_x, either a lean NO_x trap (LNT) or a selective catalytic reduction (SCR) catalyst, that reduce NO_x by using ammonia, need to be integrated into the exhaust line, according to manufacturer specifications [8]. Depending on the particular SCR coating components, these devices can be fitted to provide high NO_x conversion efficiency at low (150 – 450 ^{o}C, Cu-zeolite) or high (350 – 600 ^{o}C, Fe-zeolite) temperature ranges [9]. By contrast, LNT devices show their maximum NO_x trapping efficiency within a temperature window ranging from 250^{o}C to 450^{o}C [10], being more insensitive to NO and O_2 as the temperature increases [11].

Regarding the use of the diesel particulate filter (DPF), a powerful device for trapping particulate matter, the desired inlet temperature to reach passive regeneration condition is over 300 ^{o}C [12]. On the other hand, regeneration processes in the presence of O_2 should have initial temperature above 550 ^{o}C [13]. This could be achieved by making use of control strategies of exhaust thermal management that effectively increase the exhaust temperature [14] such as retarding the main injection timing, reducing the rail pressure set point, decreasing the boost pressure set point or adding post-injections [15].

Another issue is the trade-off relationship between NO_x and soot. The use of exhaust gas recirculation, especially low pressure EGR, leads to the reduction of combustion temperature and therefore reduces NO_x emissions [16]. Due to the low oxygen concetration at high EGR rate, soot oxidation is incomplete and thereby emission of soot increases with increasing EGR rate [17]. This action will also reduce in-cylinder peak temperature and consequently the exhaust manifold temperature, what will be adverse for aftertreatment operation.

The need of an early aftertreatment light-off during warm-up periods drives thermal management research into different perspectives. Control techniques to estimate exhaust temperature have been proposed, as remarked in the work of Guardiola *et al.* [18], who presented an in-cylinder pressure model to do so. Similarly, Gelso *et al.* [19] used the model predictive control technique to control a diesel engine and estimate several EATS parameters, including exhaust temperature. In [20], Fulton *et al.* investigated a turbine inlet exhaust temperature observer based on isentropic expansion and heat transfer across a turbocharger turbine.

Although a proper knowledge of the engine conditions is required to improve the aftertreatment performance during engine operation, turbine outlet temperature (T_4) increase is still the primary issue. However, acting on this

parameter affects other variables, being difficult to overcome the trade-off trend with brake specific fuel consumption (BSFC). Exploring the topic of exhaust temperature increase, many studies have undertaken concerns on aftertreatment performance improvement via T_4 and its penalty on engine fuel economy. D'Ambrosio *et al.* [21] designed an intake and exhaust manifold integrated in the cylinder head in order to improve the low-frequency thermal fatigue resistance on the cylinder head. This investigation resulted on a faster aftertreatment warm-up, been able to maintain the same BSFC. Galindo *et al.* [22] also proposed an optimal exhaust manifold design looking for an improved thermal behavior by reducing the pressure pulses interference during load transient operation. The results showed that a potential not only to improve the engine transient performance at low engine speeds but also the gas temperature at the catalyst inlet and the steady effective torque existed.

The turbine technology can have also a relevant impact. The topic was addressed by Verschaeren *et al.* in [23], where a 1D heavy-duty medium speed marine engine was modeled, focused on temperature increase for SCR efficiency improvement. In this work, a good compromise between exhaust temperature and fuel consumption was obtained by means of a turbine waste-gate employment, whose opening makes T_4 increase. Serrano *et al.* explored the pre-turbine DOC&DPF placement as a way to favor the pollutants oxidation and DPF passive regeneration [24] while reducing engine back-pressure and reducing the fuel penalty of the aftertreatment system [25]. In addition, this technique was shown to provide high potential for monolithic reactors downsizing [26] keeping benefits in fuel economy.

Other studies have focused on the valve timing. Basaran *et al.* [27] modulated the intake valve closing timing on a diesel engine for exhaust gas temperature increase. This method also helped improving the engine efficiency by reducing the pumping losses. Maniatis *et al.* [28] also investigated variable valve trains in combination with second exhaust valve opening as a way to increase the turbine outlet temperature, despite the trade-off with fuel specific consumption.

The studies aimed to increase the exhaust temperature show that there is room for improvement by, for example, combining different proposals with passive design solutions, such as thermal insulation. The aim of this paper is to work out further and with better tools the investigations on methods to increase the exhaust temperature, as studied by Serrano *et al.* [29], who analyzed valve timing and exhaust ports design to achieve this target. In this work, different exhaust line thermal insulation strategies are computationally investigated in a passenger car diesel engine to improve T_4 for optimum aftertreatment operation and looking at the same time for BSFC reduction. Therefore, it is fundamental to work with an accurate turbocharger heat transfer model, able to display good results for a precise study of the insulation effects on T_4. In addition, an exergy analysis is also conducted to consider the impact of the mechanical work generated by the turbine and identify the regions where thermal insulation efforts make sense. The study comprises the analysis of low and partial-high steady state operations, dealing with theoretical limits and representative technology solutions for the exhaust ports and the turbine. As a first step, different configurations are evaluated separately. Then, the most promising approaches for exhaust ports and turbine are combined and assessed in terms of T_4 and BSFC trade-off.

2. Methodology

In this work, a four-cylinder automotive diesel engine is designated to be simulated. The basic characteristics of the engine are listed in Table 1.

The engine model is built by using the commercial software GT-Power [30], a 1D engine performance simulation software. Standard GT-Power elements have been used to build up the model, except for the turbocharger, which has been replaced by an advanced sub-model developed internally in OpenWAM software [31], a free open-source 1D gas-dynamics code, created by CMT-Motores Térmicos [32, 33]. This sub-model simulates heat transfer and mechanical losses in the turbocharger, improving the prediction of the turbine outlet temperature and therefore providing more accurate results and analysis capability for the undertaken studies. More details of such model can be found in Serrano *et al.* [34]. An analysis of the turbocharger heat transfer and mechanical losses influence in the prediction of the engine performance is conducted in [35].

Figure 1 shows a schematic diagram of the energy fluxes in the turbocharger [36]. Baines *et al.* [37] state that only a fraction of the exhaust gases energy is converted across the turbine to mechanical work and transferred to the compressor. In fact, the internal heat transfer from the turbine to the bearing housing as well as the external heat transfer from the turbine to the environment are the most important losses that affect the turbocharger performance. In addition, heat flows from the gas to the turbine housing and later arrives to the compressor, worsening its efficiency [38]. Part of the heat is removed by the lubricating oil and coolant circuits while other part of the energy is exchanged between the turbocharger and the surroundings through radiation and convection. Another consideration is that, from a heat transfer modeling approach, the radial variation of temperature can be omitted, since it is negligible compared to the axial one [39].

The lumped turbocharger heat transfer model is sketched in Figure 2. It comprehends 5 internal nodes, representing the turbine housing (T), the compressor housing (C) and 3 different metal nodes for the central components. The model is completed with two external nodes representing the exhaust gas and the air. The 3 metal nodes are set between the turbine and the compressor to obtain a more precise temperature field, which presents a high gradient due to the active cooling of the components placed in there (oil and sometimes water cooling). One of the nodes is located in the hot turbine back-plate (H_1 in Figure 2); another in the cold compressor back-plate (H_3 in Figure 2); and a third one is placed in the central bearing housing (H_2 in Figure 2), where oil and water ports are located and therefore heat is usually dissipated.

The turbine extracts energy from the exhaust gas flow ($\dot{W}_{T,a}/\dot{m}_T$) between inlet turbine (IT) and outlet turbine (OT) stations. It is used to drive the compressor causing the later air enthalpy to rise. $\dot{W}_{C,a}/\dot{m}_C$ represents the specific compression work in adiabatic conditions between inlet compressor (IC) and air (A) stations. Finally, the turbocharger power balance is represented by the equation in the lower part of Figure 2, where $\dot{W}_{mech}$ is the mechanical power losses. Figure 2 shows that, in addition to work, heat is also transferred between turbine and compressor. The heat losses from the turbine ($\dot{Q}_{GAS/T}$) are transferred from the turbine case (T) to H_1 and so on until it reaches the compressor

(C). In node H_2 the heat flux is partly rejected to the lubricating and cooling systems. Regarding the compressor, it is observed that the air exchanges heat with the compressor casing ($\dot{Q}_{C,Air}/\dot{m}_C$).

In order to determine the metal conductances and to obtain an initial estimation of thermal capacitances, a thermo-hydraulic test rig is set in which, firstly, an incompressible fluid is flowed through the turbocharger [40]. Measurements in a hot flow gas stand allows obtaining the correlations for both internal heat transfer and external heat transfer. The final consideration is that the temperatures are not time but mass averaged, which results in a more accurate temperature prediction [41]. In addition, in order to adapt a mathematical model for turbocharger mechanical losses, adiabatic measurements from gas stand are performed, as discussed by Serrano *et al.* [42]. With these models, to calculate the heat transfer and mechanical losses for any operating condition of the turbocharger in the engine is possible.

The tests went through six chosen operating engine points, as shown in Table 2. These points have been selected to cover a wide range of conditions in the engine operation map. The operating points #A, #B and #C are related to low load conditions whereas #D, #E and #F represent high load, in a way that different trends and quite a few variations can be addressed.

Figure 3 shows the engine model in GT-Power, indicating the intake manifold, cylinders, exhaust manifold and turbocharger model, which are circled with a blue line. The exhaust system is highlighted and divided into 3 sections. The 1^{st} and 2^{nd} sections represent the exhaust ports. The two individual channels in the 1^{st} section merge roughly halfway through the ports, forming one larger cylindrical channel in the 2^{nd} section. The mixture is finally discharged in the exhaust manifold, represented by the 3^{rd} section.

Before carrying out the studies, a comparison between measured data and modeled results was performed to verify the model reliability. In Figure 4 this comparison is shown with focus on BSFC, fuel injected mass, T_4, air mass flow, T_3 and turbocharger speed. For all experimental conditions the same fitting coefficients have been set, reason why some operating points show greater error than others. The model provides a good balance with the experimental data as well as consistency. Despite some high relative error in air mass flow, like in point #B, in which reaches 15.5%, the model behaves coherently moving this mismatch to a corresponding impact on exhaust gas temperature prediction. Nevertheless, the absolute differences in air mass flow are kept within a narrow range, so that the impact in absolute error of T_3 and T_4 is reduced and acceptable for comparison proposals between the parametric computational studies. Complementary, Figure 5 shows the comparison between experimental and modeled in-cylinder pressure for all the operating points. As for cycle-averaged variables, in-cylinder pressure prediction is well balanced among all points providing good accuracy both during the open and closed loops, as detailed by the different zooms represented in Figure 5.

In all parametric studies, torque and intake manifold pressure are kept constant using PID controllers. Torque has been controlled by means of injected fuel quantity and the intake manifold pressure has been governed by the variable geometry turbine (VGT) opening. For low loads, the oxygen concentration resulting from the mixture between fresh air and high pressure EGR has been regulated by the EGR valve opening. For the case where oxygen concentration is

still too high even with the EGR valve fully open, an intake valve upstream the EGR and air mass flow mixing point throttles the air charge.

The temperature and the exergy evolution through the exhaust line for the six chosen operation points are displayed in Figure 6. The exhaust line positions #1, #2 and #3 in the X-axis of each chart in Figure 6 are corresponding to the positions labels with 1, 2 and 3 of the exhaust system showed in Figure 3. The points #4 and #5 represent the turbine inlet and outlet respectively. Looking at both variables evolution, it is observed an accentuated drop in the 1 st section of the exhaust manifold, then a smoother loss of temperature and exergy from point #2 to point #4 and finally an abrupt drop again in the turbine, between points #4 and #5. Exergy has been calculated according to Eq. 1:

$$Exergy_i = \dot{m}\left(h_i + \frac{{v_i}^2}{2} - T_{amb}\Delta s_i\right) \tag{1}$$

A huge difference in exergy between the dotted and the full line can be seen in the last section of the series. This difference corresponds to the exergy from mechanical power, which is only considered at the turbine outlet. The negative slope in the exergy full line series in sector #4 to #5 means that not only the expansion of the gas in the turbine reduces the temperature but a relevant exergy destruction is also taking place.

This behavior triggers an interest in reducing the temperature loss in two locations: between #1 and #2, where the exhaust ports are located, and from #4 to #5, where the active turbine cooling (oil and water) is placed. Conventional exhaust ports lose significant heat because they transport hot gas at the highest temperature from the cylinder to the exhaust manifold being water-cooled; the high temperature drop in the turbine is caused by the expansion of the exhaust gas to produce mechanical power and by wall heat transfer to the ambient and to the cooling and lubrication systems of the turbocharger bearing housing. For this reason, the parametric studies have been focused on two separate strategies, which are exhaust ports and turbine thermal insulation, to obtain less temperature drop and, as a consequence, higher T_4. At the same time it is sought to cause as little prejudice in BSFC as possible, or even to achieve some improvements on it and others engine parameters.

3. Results and discussion

3.1. Thermal insulation of the exhaust ports

The temperature sensitivity in the first section of the exhaust manifold underlines an interest for an optimum design of the exhaust ports integrating both fluid mechanics and heat transfer criteria. Therefore, this first studied strategy consists of insulating the exhaust ports, reducing their heat exchange with the surroundings. The proposed insulation corresponds to the 1st and 2nd sections in Figure 3, what comprehends exhaust port positions #1 to #3 in Figure 6. There were performed 4 different cases to accomplish this objective, which are sketched in Figure 7. Case #1 represents the baseline design. Case #2 evaluates the effect of an air chamber in the inner part of the exhaust, whilst Case #3 includes a ceramic coating between the air chamber and the exhaust pipe. Finally, for comparison effects, Case #4 corresponds to an adiabatic configuration that represents the theoretical limit.

Table 3 shows the material properties applied in the four different configurations, which includes density, thermal conductivity, specific heat and surface emissivity. Aluminum is the original material of the exhaust ports. Stainless steel is set in the inner part of the port, when an air chamber and YSZ (Yttria-stabilized zirconia), a ceramic in which zirconia (ZrO_2) is reinforced with yttria (Y_2O_3) to obtain a stable structure at room temperature [45], are added to the configuration. The thickness of each layer for every case is listed in Table 4.

Exhaust ports thermal insulation results in higher T_3 because of the heat loss reduction. This increase on T_3 makes the VGT to open, as it can be observed in Figure 8(a) and (d), for low and high load operating points respectively. Consequently, the pressure before the turbine (p_3) decreases, as shown in plots (b) and (e) in Figure 8. A decrease in p_3 also represents a benefit for pumping losses, as demonstrated in Figure 8(c) and (f). The effective efficiency is increased not only by the reduction of the pumping losses, but also because of an increment of the indicated efficiency, which is shown in Figure 9. The reason for this increment is due to the maximum in cylinder temperature decrease and, hence, the heat losses inside the cylinders.

Figure 10 displays the variation in temperature along the exhaust line for the simulated engine operation points and the described parametric study. As indicated, all the curves show higher temperature along all the exhaust system until T_4, represented by the exhaust position #5. As expected, the adiabatic curve shows the highest temperature for all operation points. The extra ceramic coating added over the air chamber, *i.e.* Case #3, provides almost no improvement in comparison with Case #2, which has only an air chamber in the inner part.

Finally, Figure 11 summarizes the variation in T_4 and BSFC compared to the baseline for the studied parametric cases. Eq. 2 and 3 express how these values are obtained:

$$\Delta T_4 = T_{4_{case\#i}} - T_{4_{baseline}} \tag{2}$$

$$\Delta BSFC[\%] = \frac{BSFC_{case\#i} - BSFC_{baseline}}{BSFC_{baseline}} \times 100 \tag{3}$$

As shown in Figure 11(a) and (c), the exhaust ports thermal insulation produces an increment of T_4 for all cases. Case #4, which represents the adiabatic condition, is the one where the highest T_4 is obtained due to the absence of heat exchange with the wall. However, Cases #2 and #3, which are realistic feasible configurations, also present a relevant increment in T_4 that ranges between 10-30 K at low load and 50-60 K at high load. This effect is due to a much lower thermal conductivity of the materials present on the two cases containing insulation than purely aluminum, which is the only material used in the exhaust port for the baseline configuration. It is possible to see that adding 1 mm of YSZ ceramic coating does not produce a significant improvement on insulation to the system, since its material properties are not as excellent as air for insulation being its effect canceled out.

Besides benefits in aftertreatment inlet temperature, fuel economy improvements are also reached, as shown in Figure 11(b) and (d). This is especially evident at high load, due to pumping losses reduction and indicated efficiency improvement, as seen in Figures 8 and 9. Figure 11 depicts that for very low load there is almost no improvement

on BSFC, in agreement with the gain on T_4, which is scarcely representative. This in agreement with p_3 and PMEP, which present a small variation in comparison to the baseline case. As load and engine speed increase, BSFC is reduced up to approximately -1.25% since PMEP and p_3 improvements are more significant for these cases.

3.2. Turbine thermal insulation

The temperature sensitivity between #4 and #5 exhaust port positions in Figure 6 also emphasizes the interest for a turbine heat exchange optimization by means of minimizing the heat loss insulating the turbine. Regarding this strategy, five cases have been defined to explore the T_4 increase, as described in Table 5. Case #1 represents the baseline design; Case #5 performs a reduction of 50% in the contact area between the turbine and the housing place; in Case #6 water cooling is suppressed and the turbine is equipped with a thermal shield; in Case #7 the turbine contains an internal ceramic coating (1 mm of YSZ material); and Case #8 represents an adiabatic turbine as a limit configuration.

Figure 12 compares the turbocharger heat transfer balance in the baseline turbocharger (turbine) configuration for the studied operating points. This is an indicator of heat power exchanged between two or more environments. For each operating point, two columns are depicted. The one on the left side represents the heat transferred from the gas flow to the walls of the turbocharger whilst the one on the right side stands for the heat transferred from the walls to the fluid flow.

Only the gas flowing across the turbine heats up the walls in low load operating points. In these cases, the walls transfer heat to fresh air in the compressor, to the water cooling flow, to the oil flow and finally to the ambient. At high load, high pressure and temperature are originated, making not only the turbine but also the compressor to transfer heat to the walls, what also makes the wall temperature to increase. Finally, the oil flow also heats up the turbocharger walls at high load since it reaches higher temperature due to higher friction losses power.

The heat transfer balance for the additional four configurations listed in Table 5 are illustrated in Figure 13. In the adiabatic case (Case #8), shown in plot (a), there is no heat transfer involving the turbine and the surroundings, so that heat only exchanges between the other mentioned fluids. For the half area case (Case #5), plot (b) evidences that although the area is decreased by half and the heat transfer is directly proportional to the surface area, the heat exchange is still very similar to the baseline case. If one compares Figure 12 with Figure 13(b) is possible to clearly see, especially in the operating point #F, how the heat flux to the ambient is proportionally increased, in spite of the heat flux to the water cooling in the bearing housing has been reduced.

Plot (c) in Figure 13 shows the configuration removing water cooling but insulating the turbine with a thermal shield (Case #8). The heat transfer to the coolant fluid is now zero since it is absent. Besides, the lubricant oil share has substantially increased compared to all previous cases, once the heat transferred to the water cooling fluid in the other cases is this time mainly moved to the oil flow. In addition, due to the thermal shield included in this configuration, the heat losses from the turbine are lower than in the baseline case. Finally, the ceramic coating case (Case #7) provides a significant reduction in the heat losses coming from the turbine. In fact, they are lower than in

the case containing thermal shield insulation, as can be seen in Figure 13(d), specially evident at high load operation points. It happens because, as defined in Table 5, the ceramic coating reduces the heat flow already through the turbine volute wall.

As shown in Figure 14(a) and (e), the heat loss reduction makes the VGT open, mainly in Case #8, since, according to Figure 13(a), the adiabatic case presents less heat losses from the turbine and there are passive changes downstream of the turbine inlet. Thus, p_3, which is represented in plots (b) and (f) for low and high loads, and the pumping losses (Figures 14(c) and (g)) are reduced.

For a final comparison, Figure 15 displays the turbine outlet temperature and BSFC variations with respect to the baseline case. X-axis represents each of the 5 parametric studies described in Table 5. It is noticed, according to the comments in the previous paragraph, that the adiabatic case reaches the highest temperature for T_4, which increases 20 to 40 K with respect to the baseline configuration. In terms of benefit, Case #7 (ceramic coating) shows the highest improvement, with 10 K increase from the baseline case. Also BSFC shows a slight improvement, mainly for the adiabatic case, with the only exception of the very low load case (point #A).

3.3. Combination of exhaust ports and turbine thermal insulation

After exposing two different strategies to achieve T_4 improvement, a possible further step to be adopted is to employ both of them at the same time, expecting to obtain a synergistic result. That said, a third study was undertaken divided into two parts. Firstly, a combination of both adiabatic cases is considered to determine the maximum value of T_4 that could be achieved using these strategies. Next, two cases that present feasible technological solutions are merged.

Table 6 shows the four compared cases for the first part of this third study. Thus, Figure 16 represents T_4 and BSFC variations for all adiabatic cases. As expected, Figure 16(a) and (c) show further improvement on temperature when both strategies are applied simultaneously. For all running points, a pronounced almost linear increase is observed, making it possible to reach up to 130 K temperature variation. Specific fuel consumption has also presented a noticeable improvement when both strategies are employed. Figures 16(b) and (d) represent BSFC values for all parametric studies and evidence that for this last study, BSFC is reduced up to 2%.

A part of the theoretical optimal case, a realistic strategy has been considered in the second part of the study, where turbine with ceramic coating in the volute is employed at the same time the exhaust ports are insulated with an air chamber. This way, the results are compared between the studies listed in Table 7. Figure 17 shows that positive results are found for the four parametric studies. With respect to T_4, plots (a) and (c) evidence that T_4 reaches up to 50 K for low load and 80 K for high load. The combination is also favorable for BSFC, with the only exception of point #A, which has already presented fuel penalty in comparison to the baseline for the turbine insulation case. For the rest, the specific fuel consumption is significantly improved around 1%.

Analyzing the results in more detail, it can be confirmed a synergistic effect, since combining both solutions produces a greater outcome than the simple sum of their individual impact. For example, analyzing operating point #D,

the sum of results for T_4 variation in turbine with ceramic coating (10 K) and exhaust ports with air chamber (50 K) is 60 K, but the actual temperature variation for the combination of both solutions is 75 K. The same phenomenon happens for almost all cases considering the BSFC variation. Therefore, it is noticed that only turbine thermal insulation produces a not so noticeable benefit. However, in the combined case with prior exhaust ports thermal insulation, T_3 is higher and p_3 is lower, maintaining the same turbine work. For operating point #B, the value for p_3 is 1.21 bar in the baseline case, 1.20 bar for Case #7, 1.18 bar for Case #2 and 1.17 bar for Case #10. This response evidences how additional benefits in T_3 increase allows the VGT to open even more. For the same operating point #B, the VGT position is 16% in the baseline case, increasing to 16.9% for the thermal insulated turbine, to 21.2% when the exhaust ports are insulated and up to 23.8% when combining both solutions in Case #10. Being the VGT more opened, the pumping losses result even more reduced and the expansion ratio in the turbine is also lower, causing a smaller drop in temperature from T_3 to T_4. Therefore, T_4 reaches a higher value compared to the baseline than adding separately the individual variations for Cases #2 and #7.

4. Summary and conclusions

This paper has presented a study willing to improve the aftertreatment boundary conditions in internal combustion engines by increasing its inlet temperature applying passive methods able to be combined to other techniques. Increasing the turbine outlet temperature represents a positive impact on the warm-up process, reducing the time for light-off of the different exhaust aftertreatment devices. It is essential to enable the aftertreatment to achieve the target conversion efficiency and reduce the requirements for particular engine warm-up or DPF active regeneration strategies.

Different approaches for exhaust line components thermal insulation have been evaluated. The results have been obtained computing a gas dynamics engine model coupled to an advanced turbocharger heat transfer and mechanical losses sub-model previously calibrated against experimental data. Through the performed studies, it has been seen that there are feasible methods to enhance the aftertreatment inlet temperature providing, moreover, reduction in specific fuel consumption. As a result, a database covering in detail the impact of exhaust ports and turbine thermal insulation is provided.

Summarizing, plots (a) and (b) in Figure 18 make it possible to classify the best and worst strategies as a function of the impact on T_4 and BSFC for each operating point. Figure 18(a) illustrates the results performed in adiabatic conditions for turbine and exhaust ports thermal insulation and also the final study, with both strategies combined. On the other hand, Figure 18(b) shows the results for feasible solutions concerning exhaust ports and turbine thermal insulation. In both plots, the top left quadrant stands for the ideal case, where T_4 increase and BSFC reduction are obtained. This region is where most of the results are concentrated. The top right quadrant denotes the cases that present temperature improvement though BSFC penalty.

It is clear that all the results for adiabatic conditions have a close to double effect than the best realistic solutions. Besides, adiabatic cases report only positive results, i.e. less specific fuel consumption and T_4 increase. Nevertheless, plot (b) in Figure 18 shows the vast majority of results on the top left of the graphic and none of them represents a decrease of T_4, meaning that all cases have significant positive impact on both merit variables. The points for the cases where turbine is insulated still present some results with negligible influence on T_4 and even some cases presenting BSFC penalty, these last related to very low load conditions. Exhaust ports thermal insulation demonstrates to be a promising strategy concerning to heat losses reduction solutions. It shows positive results for T_4 and BSFC and clearly better than the ones just focused on turbine thermal insulation, which are damaged by heat fluxes toward non-avoidable lubrication and cooling systems.

Nevertheless, the combination of both strategies produces remarkable T_4 increase and BSFC reduction, evidencing a synergistic effect governing the T_4 increment potential. Finally, the still considerable difference between the adiabatic and the feasible results leaves the way open for further optimization of thermal insulation solutions or combination between two or more methods specially looking for a previous increase in exhaust manifold temperature.

Acknowledgements

This research has been partially supported by FEDER and the Government of Spain through project TRA2016-79185-R. Additionally, the Ph.D. student Bárbara Diesel has been funded by a grant from the Government of Generalitat Valenciana with reference ACIF/2018/109.

[1] Johnson TV, Joshi A. Review of vehicle engine efficiency and emissions, SAE Technical Paper 2018-01-0329; 2018, doi:10.4271/2018-01-0329.

[2] Commission Implementing Regulation (EU) ../.. of 2.6.2017 setting out a methodology for determining the correlation parameters necessary for reflecting the change in the regulatory test procedure with regard to light commercial vehicles and amending Implementing Regulation (EU) No 293/2012 (June 2017).

[3] Ko J, Jin D, Jang W, Myung CL, Kwon S, Park S. Comparative investigation of NOx emission characteristics from a Euro 6-compliant diesel passenger car over the NEDC and WLTC at various ambient temperatures, Appl Energy 2018; (187):652-662.

[4] Li T, Yin T, Wang B. Anatomy of the cooled EGR effects on soot emission reduction in boosted spark-ignited direct-injection engines, Appl Energy 2017; 190:43-56.

[5] Stojkovica BD, Fansler TD, Drake MC, Sick V. High-speed imaging of OH* and soot temperature and concentration in a stratified-charge direct-injection gasoline engine, Proc Combust Inst 2005; 2657-65.

[6] Hamedi MR, Doustdar O, Tsolakis A, Hartland J. Thermal energy storage system for efficient diesel exhaust aftertreatment at low temperatures, Appl Energy 2019; 235:874-887.

[7] Payri F, Arnau FJ, Piqueras P, Ruiz MJ. Lumped approach for flow-through and wall-flow monolithic reactors modelling for real-time automotive applications, SAE Technical Paper 2018-01-0954; 2018, doi:10.4271/2018-01-0954.

[8] Dardiotis C, Martini G, Marotta A, Manfredi U. Low-temperature cold-start gaseous emissions of late technology passenger cars, Appl Energy 2013; 111:468-478.

[9] Nova I, Tronconi E. Urea-SCR technology for deNOx aftertreatment of diesel exhausts. New York: Springer; 2014. ISBN 978-1-4899-8071-7.

[10] Xu L, McCabe RW. LNT + in situ SCR catalyst system for diesel emissions control, Catal Today 2012; 184:83-94.

[11] Watling TC, Bolton PD, Swallow D. The effect of NO and O_2 concentration on NO_x storage over a lean NO_x trap: An experimental and modelling study, Chem Eng Sci 2018; 178:312-323.

[12] Müller J, Frank B, Jentoft R, Schlögl R, Su D. The oxidation of soot particulate in the presence of NO_2, Catal Today 2012; 191(1):106-111.

[13] Lee SJ, Jeong SJ, Kim WS. Numerical design of the diesel particulate filter for optimum thermal performances during regeneration, Appl Energy 2009; 86:1124-1135.

[14] Shuzhan B, Guobin C, Qiang S, Guihua W, Guo-xiang L. Influence of active control strategies on exhaust thermal management for diesel particular filter active regeneration, Appl Therm Eng 2017; 119:297-303.

[15] Stenning L. Strategies for achieving pre DPF regeneration temperatures using in cylinder post injection on a common rail diesel engine with EGR, DOC and intake throttle, SAE Technical Paper 2010-36-0306; 2010, doi:10.4271/2010-36-0306.

[16] Lattimore T, Wang C, Xu H, Wyszynski ML, Shuai S. Investigation of EGR effect on combustion and PM emissions in a DISI engine, Appl Energy 2016; 161:256-267.

[17] Thangaraja J, Kannan C. Effect of exhaust gas recirculation on advanced diesel combustion and alternate fuels - A review, Appl Energy 2016; 180:169-184.

[18] Guardiola C, Olmeda P, Pla B, Bares P. In-cylinder pressure based model for exhaust temperature estimation in internal combustion engines, Appl Therm Eng 2017; 115:212-220.

[19] Gelso ER, Dahl J. Diesel engine control with exhaust aftertreatment constraints, IFAC-PapersOnLine 2017; 50(1):8921-8926.

[20] Fulton B, Van Nieuwstadt M, Petrovic S, Roettger D. Exhaust manifold temperature observer model, SAE Technical Paper 2014-01-1155; 2014, doi:10.4271/2014-01-1155.

[21] D'Ambrosio S, Ferrari A, Spessa E, Magroa L, Vassallo A. Impact on performance, emissions and thermal behaviour of a new integrated exhaust manifold cylinder head Euro 6 diesel engine, SAE Technical Paper 2013-24-0128; 2013, doi:10.4271/2013-24-0128.

[22] Galindo J, Luján JM, Serrano JR, Dolz V, Guilain S. Design of an exhaust manifold to improve transient performance of a high-speed turbocharged diesel engine, Exp Therm Fluid Sci 2004; 28:863-875.

[23] Verschaeren R, Verhelst S. Increasing exhaust temperature to enable after-treatment operation on a two-stage turbo-charged medium speed marine diesel engine, Energy 2018; 147:681-687.

[24] Luján JM, Serrano JR, Piqueras P, García-Afonso Ó. Experimental assessment of a pre-turbo aftertreatment configurations in a single stage turbocharged diesel engine. Part 2: Transient, Energy 2015; 80:614-627.

[25] Luján JM, Bermúdez V, Piqueras P, García-Afonso Ó. Experimental assessment of a pre-turbo aftertreatment configurations in a single stage turbocharged diesel engine. Part 1: Steady-state, Energy 2015; 80:599-613.

[26] Serrano JR, Climent H, Piqueras P, Angiolini E. Analysis of fluid-dynamic guidelines in diesel particulate filter sizing for fuel consumption reduction in post-turbo and pre-turbo placement, Appl Energy 2014; 132:507-523.

[27] Basaran HU, Ozsoyosal OA. Effects of application of variable valve timing on the exhaust gas temperature improvement in a low-loaded diesel engine, Appl Therm Eng 2017; 122:758-767.

[28] Maniatis P, Wagner U, Koch T. A model-based and experimental approach for the determination of suitable variable valve timings for cold start in partial load operation of a passenger car single-cylinder diesel engine, Int J Engine Res 2019, published online, doi.org/10.1177/1468087418817119.

[29] Serrano JR, Piqueras P, Navarro R, Gómez J, Michel M, Thomas B. Modelling analysis of aftertreatment inlet temperature dependence on exhaust valve and ports design parameters, SAE Technical Paper 2016-01-0670; 2016, doi:10.4271/2016-01-0670.

[30] GAMMA Technologies, www.gtisoft.com [accessed 25 May 2018].

[31] OpenWAM webpage, CMT-Motores Tèrmicos, Universitat Politècnica de València, www.openwam.org [accessed 25 May 2018].

[32] Galindo J, Serrano JR, Arnau FJ, Piqueras P. Description and analysis of a one-dimensional gas-dynamic model with independent time discretization In: Proceedings of the Spring Technical Conference of the ASME Internal Combustion Engine Division 2008; Chicago, Illinois, USA.

[33] Galindo J, Serrano JR, Arnau FJ, Piqueras P. Description of a semi-independent time discretization methodology for a one-dimensional gas dynamics model, J Eng Gas Turbine Power 2009; 131(3):034504-9.

[34] Serrano JR, Olmeda P, Arnau FJ, Dombrovsky A, Smith L. Analysis and methodology to characterize heat transfer phenomena in automotive turbochargers, J Eng Gas Turbine Power 2015; 137(2):021901-12.

[35] Serrano JR, Olmeda P, Arnau FJ, Dombrovsky A. Turbocharger heat transfer and mechanical losses influence in predicting engines performance by using one-dimensional simulation codes, Energy 2015; 86:204-218.

[36] Burke RD, Olmeda P, Arnau FJ, Reyes-Belmonte M. Modelling of turbocharger heat transfer under stationary and transient conditions, 11th International Conference on Turbochargers and Turbocharging; 2014 May 13-14; London, UK.

[37] Baines N, Wygant KD, Dris A. The analysis of heat transfer in automotive turbochargers, J Eng Gas Turbine Power 2010; 132(4):042301-9.

[38] Olmeda P, Dolz V, Arnau FJ, Reyes-Belmonte MA. Determination of heat flows inside turbochargers by means of a one dimensional lumped model, Math Comput Model 2013; 57:1847-1852.

[39] Romagnoli, A. and Martinez-Botas R. Heat transfer analysis in a turbocharger turbine: An experimental and computational evaluation, Appl Therm Eng 2012; 38:58-77.

[40] Serrano JR, Olmeda P, Páez A, Vidal F. An experimental procedure to determine heat transfer properties of turbochargers, Meas Sci Technol 2010; 21(3):035109-23.

[41] Caton JA. Comparisons of Thermocouple, time-averaged and mass-averaged exhaust gas temperatures for a spark-ignited engine, SAE Technical Paper 820050; 1982, doi:10.4271/820050.

[42] Serrano JR, Olmeda P, Tiseira A, García-Cuevas LM, Lefebvre A. Theoretical and experimental study of mechanical losses in automotive turbochargers, Energy 2013; 55:888-898.

[43] Marr MA. An investigation of metal and ceramic thermal barrier coatings in a spark-ignition engine: University of Toronto; 2009.

[44] Alaruri S, Bianchini L, Brewington A. Effective spectral emissivity measurements of superalloys and YSZ thermal barrier coating at high temperatures using a 1.6 μm single wavelength pyrometer, Opt Lasers Eng 1998; 30:77-91.

[45] Viazzi C, Deboni A, Ferreira JZ, Bonino JP, Ansart F. Synthesis of yttria stabilized zirconia by solgel route: influence of experimental parameters and large scale production, Solid State Sciences 2006; 8:1023-1028.

Definitions/Abbreviations

A	air node
BSFC	brake specific fuel consumption
C	compressor
GAS	exhaust gas node
H_1	1^{st} internal node between turbine and compressor
H_2	2^{nd} internal node between turbine and compressor
H_3	3^{rd} internal node between turbine and compressor
h	specific enthalpy
IC	compressor inlet
IT	turbine inlet
$\dot{m}$	mass flow
OC	compressor outlet
OC_s	isentropic compressor outlet
OT	turbine outlet
OT_s	isentropic turbine outlet
p_3	turbine intake pressure
$\dot{Q}$	heat flow
PMEP	pumping mean effective pressure
$\dot{Q}$	heat flux
s	specific entropy
T	turbine
T	temperature
T_3	turbine inlet temperature
T_4	turbine outlet temperature
v_i	fluid velocity
$\dot{W}$	power
W	water

Acronyms

1D	one-dimensional
DOC	diesel oxidation catalyst
DPF	diesel particulate filter
EATS	exhaust aftertreatment system
EGR	exhaust gas recirculation
HSDI	high speed direct injection
LNT	lean NO_x Trap
SCR	selective catalytic reduction
VGT	variable geometry turbine
YSZ	Yttria-stabilized Zirconia
WLTP	Worldwide Harmonized Light Vehicles Test Procedure

Subscripts

a	adiabatic conditions
Amb	ambient
B	bearing
B/Amb	refers to heat flux transferred between the bearing and the ambient
B/C	refers to heat flux transferred between the bearing and the compressor housing
B/Oil	refers to heat flux transferred between the bearing and the oil circuit
C	compressor
C/Air	refers to heat flux transferred between the compressor and the air
C/Amb	refers to flux transferred between the compressor and the ambient
Gas/T	refers to heat flux transferred between the exhaust gas and the turbine housing
mech	refers to mechanical losses
Oil	oil node
s	isentropic
T	turbine
T/Amb	refers to heat flux between the turbine and the ambient
T/B	refers to heat flux between the turbine and the bearing

List of Tables

List of Figures

- Figure 17 - Aftertreatment inlet temperature and BSFC variation at low and high load operating points as a function of different feasible exhaust ports and turbine thermal insulation configurations.
- Figure 18 - Summary of impact on T_4 and BSFC of (a) adiabatic cases and (b) feasible solutions for exhaust ports and turbine thermal insulation.

Table 1: Engine specifications of simulated engine.

Type	Turbocharged HSDI diesel
Displacement	1997 [cm^3]
Bore	85 [mm]
Stroke	88 [mm]
Number of cylinders	4 in line
Number of intake valves	2 per cylinder
Number of exhaust valves	2 per cylinder
Turbocharger model	VGT
Compression ratio	15.5:1
Maximum power @ speed	120 [kW] @ 3750 [rpm]
Maximum torque @ speed	340 [Nm] @ 2000 [rpm]
EGR type	Cooled, high pressure with intake throttle

Table 2: Identification of simulated engine points.

Point ID	Speed [rpm]	Load [%]
#A	1500	10
#B	1500	25
#C	2000	25
#D	1250	75
#E	2000	75
#F	3500	100

Table 3: Thermal properties of the exhaust ports materials.

Material [-]	Color [-]	Density [kg/m^3]	Thermal conductivity [W/mK]	Specific heat [J/kgK]	Surface emissivity [-]
Stainless steel	Black	7900	25.4	611	0.85
Air	Blue	1.1614	0.0667	1141	-
YSZ	Red	4950 [43]	1.2 [43]	490 [43]	0.729 [44]
Aluminum	Grey	2700	204	240	0.8

Table 4: Layer thickness in exhaust ports thermal insulation configuration.

	Thickness [mm]			
Case	Stainless steel	Air	YSZ	Aluminium
#1 (baseline)	0	0	0	15
#2	3	2	0	10
#3	3	2	1	9
#4	Adiabatic			

Table 5: Turbine thermal insulation cases.

Case #1	-	Baseline
Case #5	-	Contact area between turbine and housing plate 50% reduced
Case #6	-	Turbine without water cooling and with thermal shield
Case #7	-	Turbine with internal ceramic coating in the volute (1 mm YSZ)
Case #8	-	Adiabatic turbine

Table 6: Adiabatic exhaust ports and turbine cases.

Case #1	-	Baseline
Case #4	-	Adiabatic exhaust ports
Case #8	-	Adiabatic turbine
Case #9	-	Adiabatic exhaust ports and turbine combination

Table 7: Feasible cases for exhaust ports and turbine thermal insulation.

Case #1	-	Baseline
Case #2	-	Exhaust ports with an air chamber
Case #7	-	Turbine with internal ceramic coating in the volute (1 mm YSZ)
Case #10	-	Case #2 and Case #7 combination

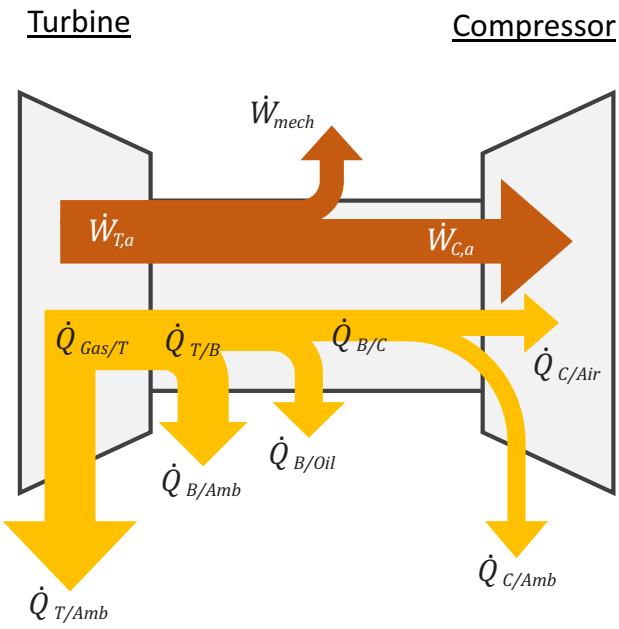

Figure 1: Energy fluxes inside a turbocharger.

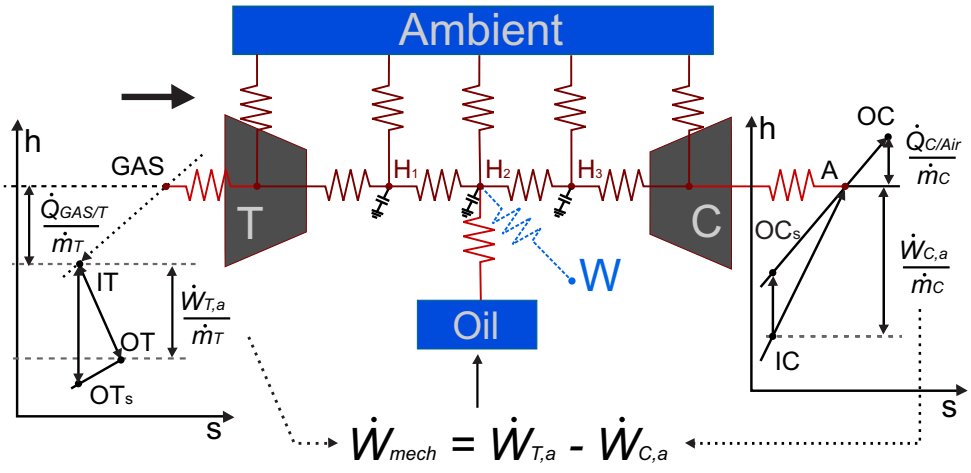

Figure 2: Scheme of the lumped turbocharger heat transfer model.

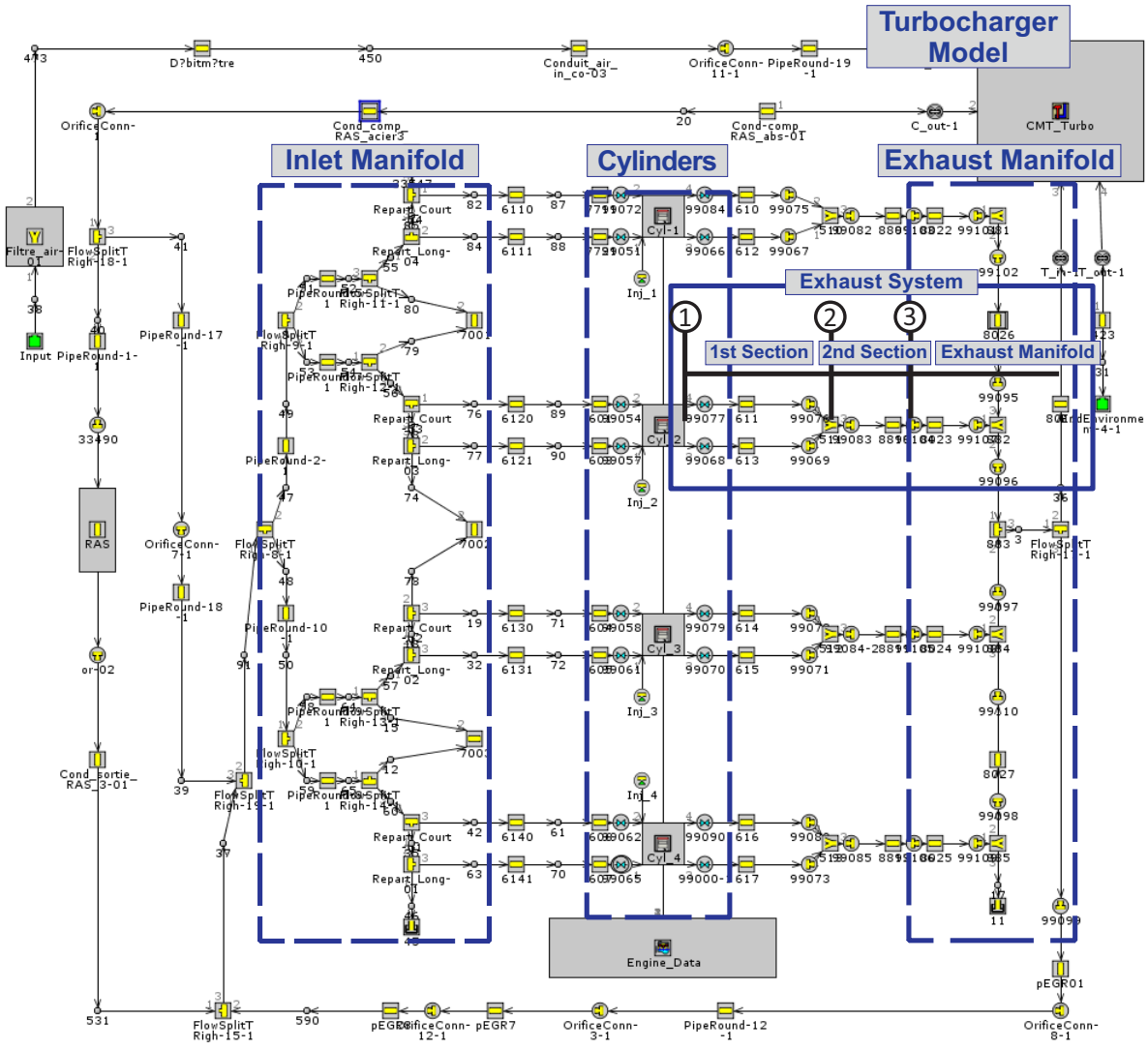

Figure 3: Scheme of the engine model in GT-Power.

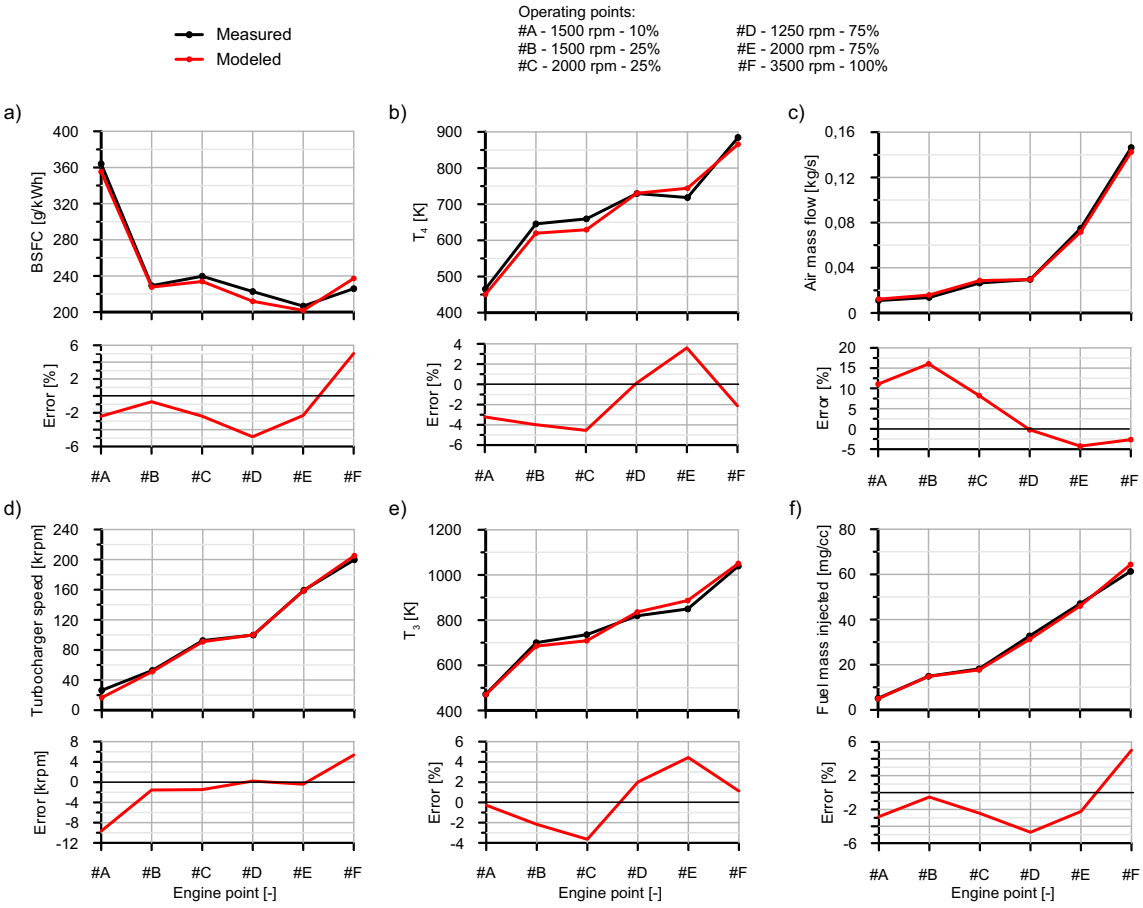

Figure 4: Comparison between experimental data and modeled results for the selected operating points.

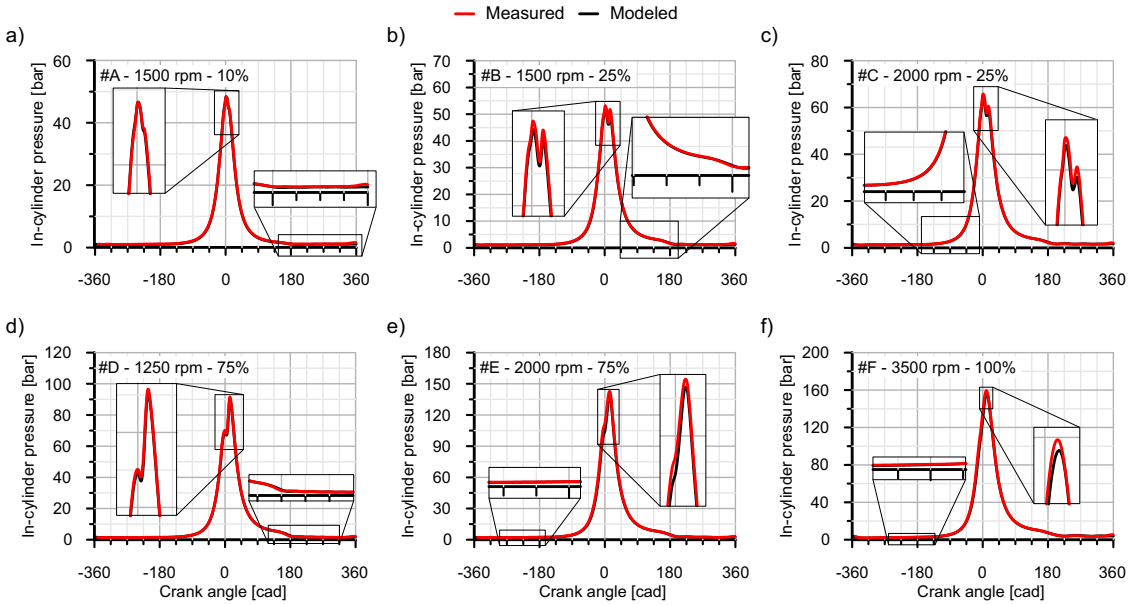

Figure 5: Comparison between experimental and modeled in-cylinder pressure for the selected operating points.

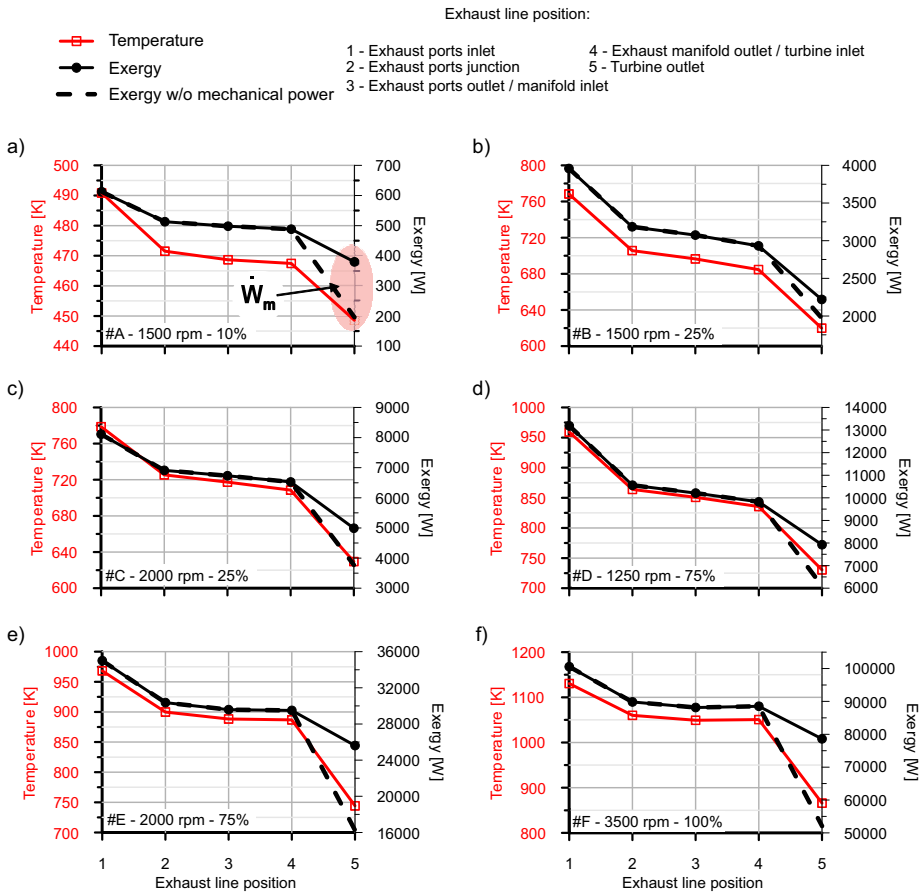

Figure 6: Temperature and exergy variation across the exhaust line in the baseline configuration.

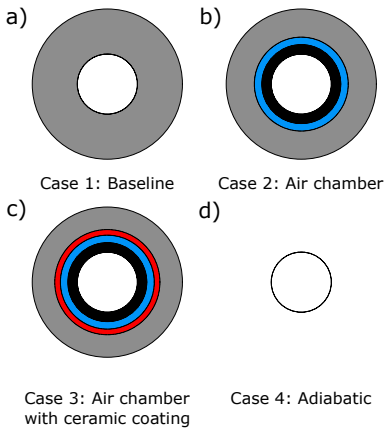

Figure 7: Representation of exhaust ports thermal insulation cases.

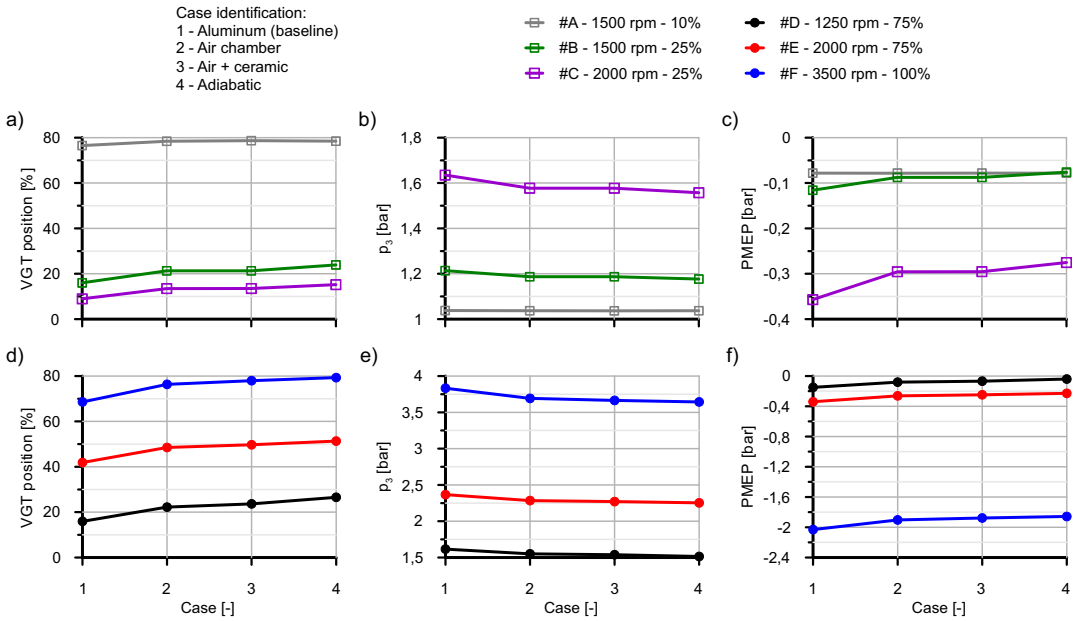

Figure 8: VGT position, inlet turbine pressure and PMEP at low and high load operating points as a function of the exhaust ports thermal insulation configuration.

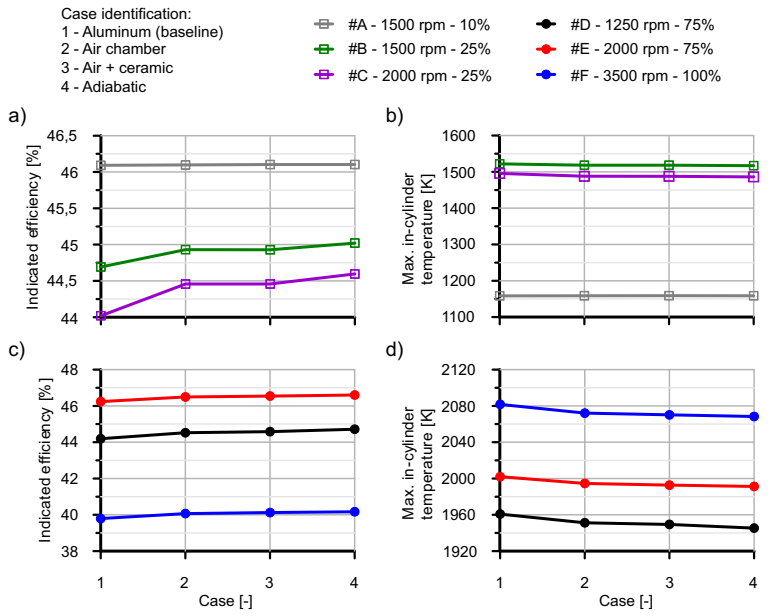

Figure 9: Indicated efficiency and maximum in-cylinder temperature at low and high load operating points as a function of the exhaust ports thermal insulation configuration.

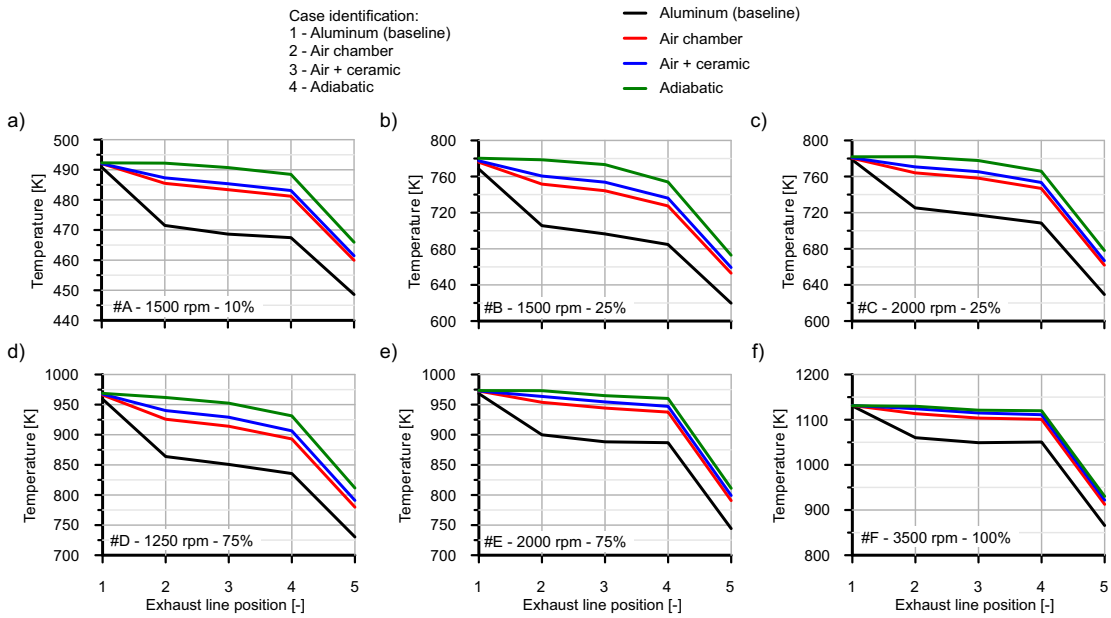

Figure 10: Temperature variation across the exhaust line as a function of the exhaust ports thermal insulation configuration.

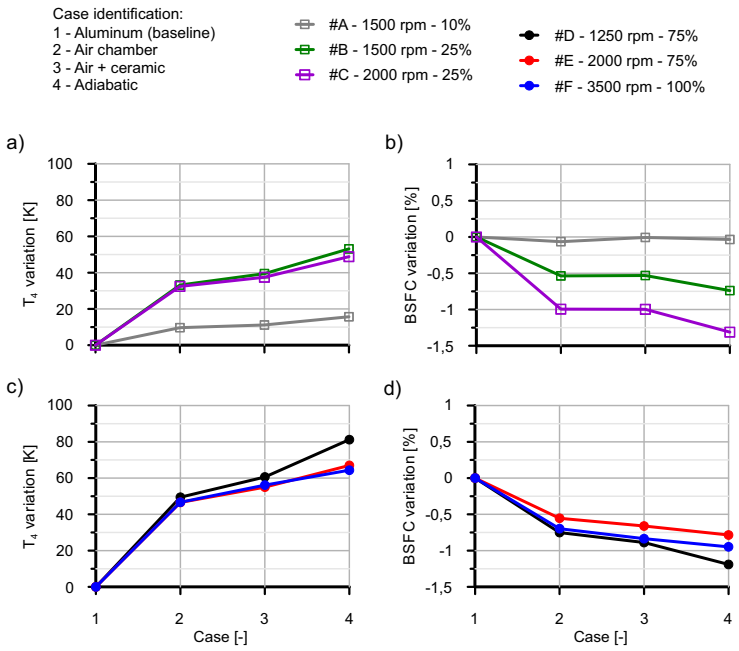

Figure 11: Aftertreatment inlet temperature and BSFC variation at low and high load operating points as a function of the exhaust ports thermal insulation configuration.

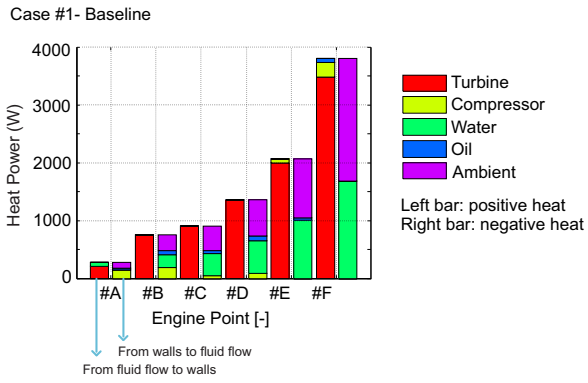

Figure 12: Heat power balance in the turbocharger for the baseline configuration (Case #1).

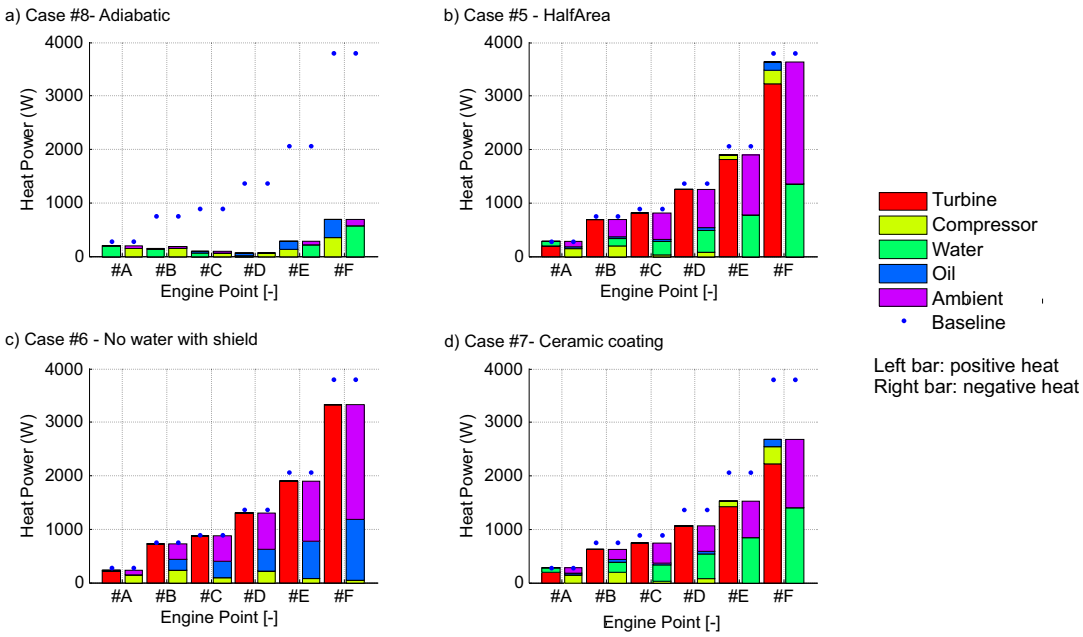

Figure 13: Heat power balance in the turbocharger as a function of the turbine thermal insulation configuration.

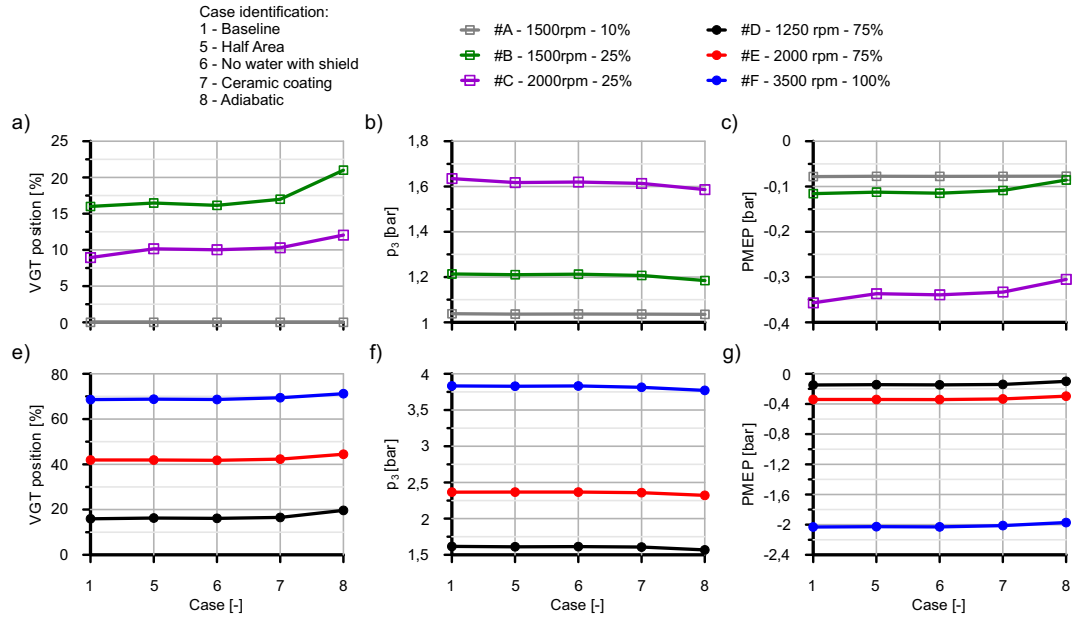

Figure 14: VGT position, inlet turbine pressure and PMEP at low and high load operating points as a function of the turbine thermal insulation configuration.

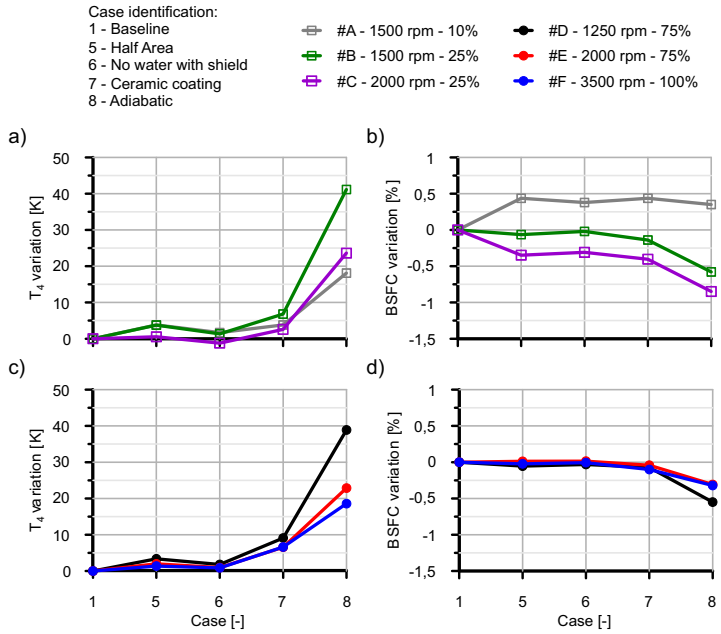

Figure 15: Aftertreatment inlet temperature and BSFC variation at low and high load operating points as a function of the turbine thermal insulation configuration.

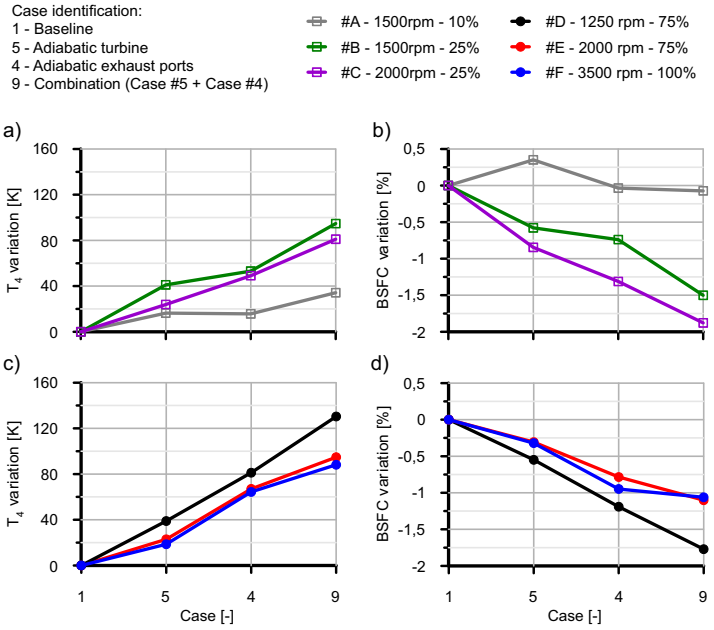

Figure 16: Aftertreatment inlet temperature and BSFC variation as a function of different adiabatic configurations in the exhaust ports and the turbine.

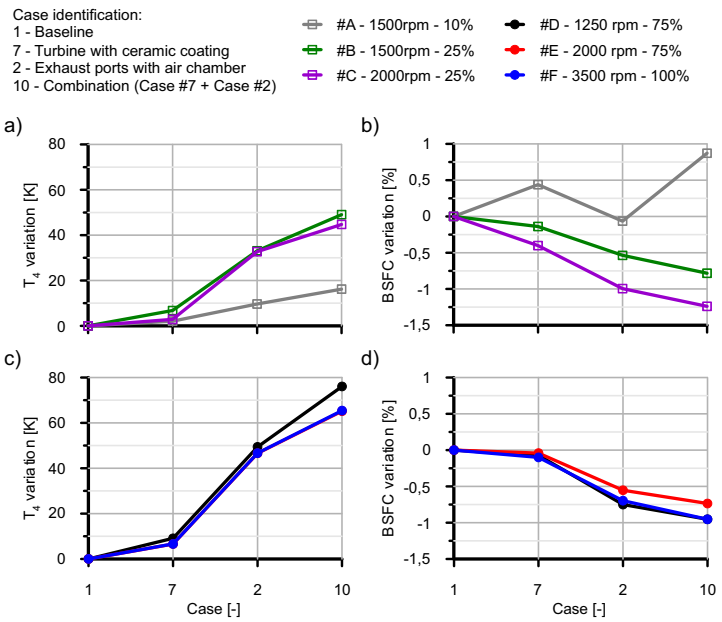

Figure 17: Aftertreatment inlet temperature and BSFC variation at low and high load operating points as a function of different feasible exhaust ports and turbine thermal insulation configurations.

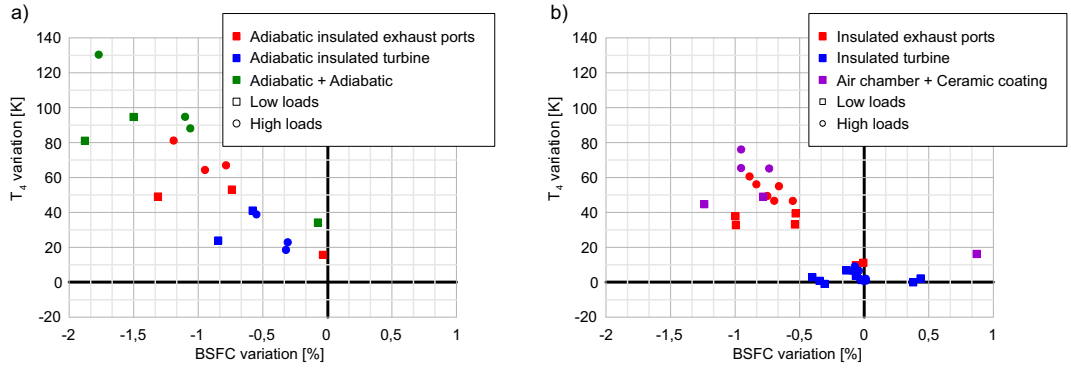

Figure 18: Summary of impact on T_4 and BSFC of (a) adiabatic cases and (b) feasible solutions for exhaust ports and turbine thermal insulation.